Mixing and Combustion Performances of a Baffle-Plate-Type Miniature Confined Multijet

Kazuya Tatsumi[1,2], Yasuhiro Rai[1], Yusuke Nibayashi[1] and Kazuyoshi Nakabe[1,2]

1: Mechanical Engineering and Science, Kyoto University,
Sakyo-Ku, Kyoto 606-8501, Japan
2: Advanced Research Institute of Fluid Science and Engineering, Kyoto University
Nishigyo-Ku, Kyoto 615-8530, Japan
tatsumi@me.kyoto-u.ac.jp

ABSTRACT

The mixing and combustion performances of a baffle-plate-type millimeter-scale confined multijet were investigated experimentally by measuring the blow-off limit of the flames, exhaust gas components and two-dimensional unburned flow velocity profiles in the chamber. Two types of multijet, parallel- and swirl-type nozzles, were examined in this study. In the parallel-type multijet case, a small change in the distance between the fuel and air nozzles showed significant effects on the blow-off limit. When the air nozzles were closely located around the center of the chamber, the flame was easily extinguished and a pair of elongated flow recirculation was observed near the chamber sidewalls. When the distance was increased, the reverse flows were observed in the central region that led to a stable and efficient combustion. In the swirl-type multijet case, the swirl made the flame to be more stable. Some cases of excessive swirl, however, deteriorate the fuel-and-air mixing performance and increase the CO concentration.

1. INTRODUCTION

Fluid mixing is one of the most important processes in fluid engineering and is applied in numerous industrial applications such as chemical processing in reactors, fuel-oxidizer mixing in combustors, and high/low temperature fluids mixing in air conditioners. There is an increase in the demand for developing a new mixing technique that has high mixing efficiency and requires compact mixing chambers. One of the important issues attributed to the decrease of the characteristic length of the combustor is the decrease of the flow Reynolds number, *Re*. When the Reynolds number decreases, the flow becomes laminar that will lead to a deterioration of fluid mixing attributed to the lack of turbulence diffusion and mixing. This will incur incomplete combustion reactions in the combustor, and exhausts of carbon monoxide and soot.

In order to tackle this problem, the authors previously proposed a miniature combustor consisted of a baffle-plate with multiple jet-nozzles (cf. Fig. 1 (a) and 1 (b)). The central nozzle, from which the fuel is supplied, is surrounded axisymmetrically by six jets, from which the oxidizer is supplied. Choi et al. [1] experimentally evaluated the flame characteristics of the multijet combustor and showed that the flame length can be decreased markedly without impairing the stability even under fuel-lean conditions. Woodfield et al. [2] carried out a three-dimensional numerical simulation for this baffle-plate type multijet combustor under low *Re* condition in the range of $50 < Re < 200$. They showed that fluid mixing between the central and surrounding jets is increased compared with the conventional co-axial jet case. This was attributed to the reverse flow generated at the downstream of the central jet caused by the momentum difference between the central and surrounding jets. Yahagi et al. [3] studied the influence of the central/surrounding jet mass flow ratio mainly by changing the diameter of the nozzles.

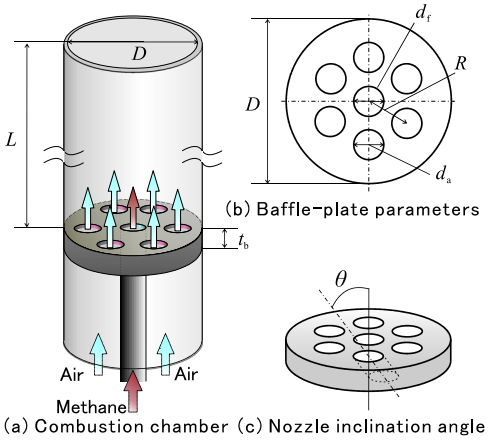

Fig. 1 Schematic of baffle-plate type multijet

In this study, two types of the multijet combustors are discussed. One is a multijet similar to those mentioned above that has surrounding jets flowing parallel to the central jet (parallel-type). The other is a swirl-type, which has the same shape with the parallel-type except that the surrounding nozzles are inclined in the circumferential direction (cf. Fig. 1(c)). To examine the mixing performance of the swirl type before combustion experiments, Tatsumi et al. [4] carried out numerical simulations and predicted that a strong swirl can be produced by the inclined surrounding jets. The swirl not only generated a reverse flow at the chamber centerline to enhance the fluid mixing in some degree, but also made the flow stable.

In the present experiment, the measurements of flame

Table 1 Experimental conditions.

Case	R60-s0	R75-s0	R60-s20	R60-s40	R75-s20
R [mm]	6	7.5	6	6	7.5
θ [°]	0	0	20	40	20
Sw	0	0	0.20	0.46	0.25

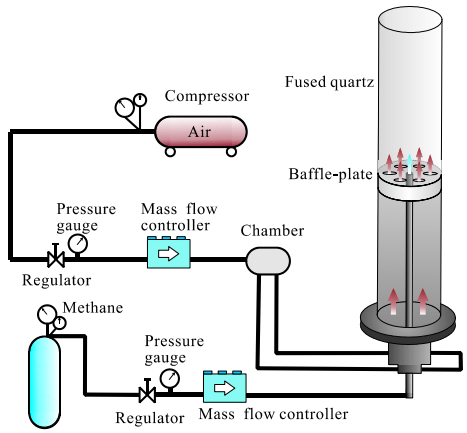

Fig. 2 Experimental apparatus.

blow-off condition, flow velocity and exhaust gas component are carried out. The effects of the radial position of the surrounding nozzles in the parallel-type case, and the inclination angle in the swirl-type case on the combustion and flow performances are discussed.

2. EXPERIMENTAL METHOD

2.1 Experimental apparatus

Figure 2 shows the experimental apparatus. Methane was used as fuel, and was supplied to the central nozzle of the baffle-plate. Air was supplied to the surrounding nozzles as oxidizer. Mass flow rates of these gases were controlled by mass flow controllers (Yamatake Co., MQV0020 and MQV0200), respectively. A tube made of fused quartz with the length of L = 300mm was placed at the downstream of the baffle-plate as the combustion chamber.

The dimensions of the baffle-plate are shown in Fig. 1 (b) and Table 1. The position of the surrounding nozzle, R, and the inclination angle of the nozzle in the swirl-type multijet, θ, were varied in this study: R = 6.0mm or 7.5mm and θ = 0° (no swirl), 20°, or 40°. The other values were kept constant; d_f = 4mm, d_a = 4mm, D = 22mm, and t_b = 7mm. In the swirl-type case, the nozzles were made so that the holes were inclined in the circumferential direction against the chamber axis as shown in Fig. 1 (c). The diameter of the hole in the baffle-plate was kept as d_a = 4mm, therefore, the shape of the nozzle exit was elliptic.

Sw in Table 1 is the swirl number defined as $Sw = 2G_a/G_tD$. G_a [kg·m^2/s^2] and G_t [kg·m/s^2] are the angular momentum and the translation momentum of the surrounding jet, respectively. Here, we ignored the momentum of the central jet because of its relatively small mass flow rate, and assumed the flow of the surrounding jet are all supplied along the centerline of the nozzle in the computation.

2.2 Measurement of blow-off condition

In order to evaluate the flame stability, blow-off condition of the combustion was measured in this study. Measurement was made by first setting the mass flow rate of the fuel, Q_f, to a certain value, and igniting at a relatively small air flow rate. The fuel flow rate Q_f was varied in the range from 0.5L/min ≤ Q_f ≤ 2.5L/min during the blow-off measurements.

While keeping Q_f constant, the mass flow rate of the air Q_a [L/min] was increased every 5s at the rate of 1L/min until the flame blew off. The blow-off limit was defined when the flame blew off at a certain air flow rate Q_a for each Q_f.

2.3 Gas mixture components analysis

The mixture components of the exhaust gas were analyzed by using a gas chromatograph (Shimadzu, Co. GC-8A). Sample gas was collected by a vacuum bottle, which was connected to a sampling tube and probe inserted into the combustion chamber. The tube was made of stainless steel, and its inner and outer diameters were 6 and 4mm, respectively. The diameter of the probe installed inside the sampling tube was 0.2mm to freeze gaseous reactions. The sampling tube was connected to a tube packed with silica gel, which was placed upstream of the vacuum bottle to remove the vapor from the sampling gas.

The sampling gas was collected at the three radial location, $|r|$ < 2mm, 2mm < r < 6mm, and 6mm < r at the streamwise location of 30mm upstream the exit of the combustion chamber. Flow velocity distributions at these positions were measured with the PIV (particle image velocimetry) system. The average values of the gas concentration were calculated by first multiplying the concentration with the flow rate at each measuring positions, and then dividing it with the total flow rate of the chamber.

The gas components of N_2, CO, and CO_2 were measured in this study. In the discussed shown in the Section 3, the following two values, reaction rate α and preferential generation rate of CO, γ, will be considered.

$$\alpha = \frac{Q_{CO} + Q_{CO_2}}{Q_{CH_4}} \quad (1)$$

$$\gamma = \frac{Q_{CO}}{Q_{CO} + Q_{CO_2}} \quad (2)$$

Q_{CO} [L/min], Q_{CO2} [L/min], and Q_{CH4} [L/min] are the volume flow rate of CO, CO_2 and CH_4 included in the exhaust gas, respectively. α is increased as CH_4 is consumed in the reaction. γ shows a smaller value as the complete combustion reactions occur in the combustor.

2.4 PIV measurement

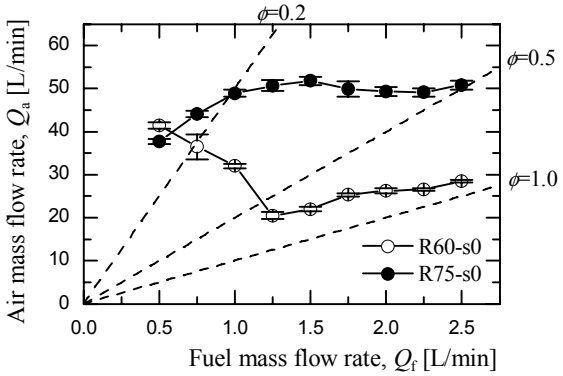

Fig. 3 Blow-off limit in parallel-type multijet case.

Flow velocity distributions in the area close to the baffle-plate were measured using the PIV method. It should be noted that the measurement was made for a non-combustion state, in which air was supplied from the central and surrounding nozzles. Therefore, the influences of the buoyancy and fluid property variation due to the temperature and gas component change are not considered. This may lead to some discrepancy with the practical flow field in the combustion. However, we believe that the results will provide some insight into the understanding of the flow characteristics in the baffle-plate type multijet combustor.

The PIV system is composed of a double pulse Nd:YAG laser (New Wave Research Solo3) and high resolution CCD camera (TSI, Powerview Plus, 4MP). The laser light was shaped in sheet form. This light sheet was aligned with the y and z axes during the measurement in order to measure the velocity fields at the x-y and x-z planes, respectively. The frame rate was 15frames/s and a sufficient number of frames of instantaneous particle image were taken to calculate the time mean velocity field. PIV analysis software (TSI, Insight 6.0) was used to obtain the flow velocity from the recorded images. When the PIV measurement was conducted, a particle generator (TSI, model 9306) was installed in the upstream of the settling chamber, and a small amount of oil mist (Di-Ethyl-Hexyl-Sebacate, 1.0μm in nominal diameter) was supplied into the air as tracing particles.

3. RESULTS AND DISCUSSION

3.1 Parallel-type multijet case

In this section, the discussion will be made on the results of the parallel-type multijet cases, R60-s0 and R75-s0, to evaluate the effect of the distance between the fuel and air nozzles, R = 6.0mm or 7.5mm under no swirl condition. The air nozzles are not inclined and are parallel to the x-axis.

Figure 3 shows the blow-off conditions in the cases of R60-s0 and R75-s0. The dash line shown in the figure presents a constant equivalent ratio, ϕ, for the corresponding conditions of Q_f and Q_a. In R60-s0 case (open circle), a relatively stable flame is observed even for lean combustion conditions of $\phi < 0.2$ when the fuel flow rate Q_f is small. As Q_f increases, the air flow rate Q_a of the blow-off limit decreases markedly showing the deterioration of the flame stability. The blow-off limit will then increase moderately along the line of $\phi < 1.0$.

In R75-s0 case, the blow-off limit with the Q_f = 0.5L/min condition shows a similar value with the one observed in R60-s0 case. The blow-off limit, on the contrary to R60-s0, increases as Q_f increases. Then, the blow-off limit remains nearly constant in the range of $\phi >$ 0.2. Comparing the above two results, it can be concluded that a higher combustion stability is obtained in R75-s0 case than in R60-s0 case.

Figures 4 and 5 show the contour maps of the streamwise velocity U and velocity vectors at the x-y and

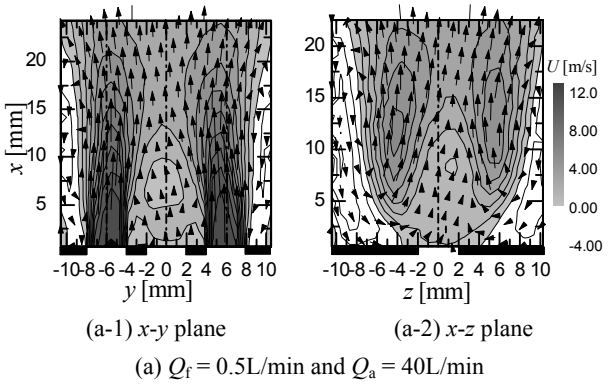

(a-1) x-y plane (a-2) x-z plane

(a) Q_f = 0.5L/min and Q_a = 40L/min

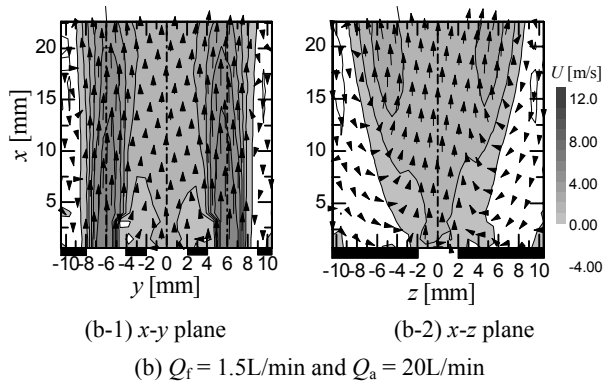

(b-1) x-y plane (b-2) x-z plane

(b) Q_f = 1.5L/min and Q_a = 20L/min

Fig. 4 Streamwise velocity U contours and velocity vectors in R60-s0 case.

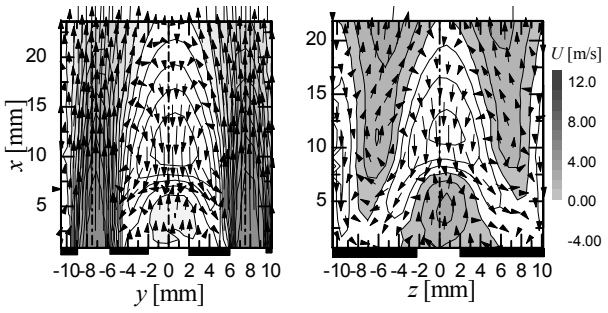

(a) x-y plane (b) x-z plane

Fig. 5 Streamwise velocity U contours and velocity vectors in R75-s0 case (Q_f = 1.5L/min and Q_a = 40L/min).

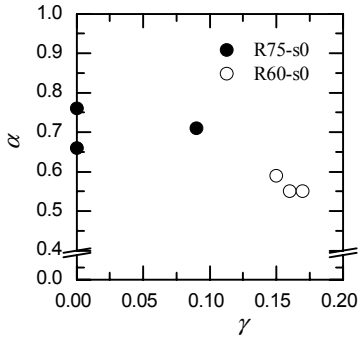

Fig. 6 Reaction rate, α, and preferential generation rate of CO, γ, in the cases of parallel-type multijet (Q_f = 0.5L/min and Q_a = 30L/min).

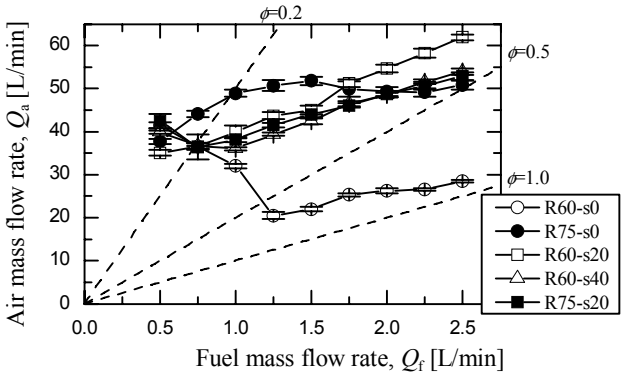

Fig. 7 Blow-off limit in swirl-type multijet case.

x-z planes. Figure 4 shows the results of two different mass flow rate conditions, (a) Q_f = 0.5L/min and Q_a = 40L/min and (b) Q_f = 1.5L/min and Q_a = 20L/min, in R60-s0 case, while Fig. 5 shows the results of R75-s0 case.

In Fig. 4 (a-1), *U* shows positive values in the area between the surrounding jets. On the other hand, near the sidewalls of the combustion chamber, the areas with negative *U* are observed showing that a reverse flow is generated in this area. In the flow distribution at the *x-z* plane that crosses between the air jets as shown in Fig. 4 (a-2), the area size of the reverse flow increases, and a radial flow heading toward the chamber centerline is observed near the surface of the baffle-plate. These results show that a portion of the surrounding jets flows upstream toward the baffle-plate along the sidewalls, and then heads toward the chamber centerline. The flow will then mix with the central jet.

Although not shown here, the transition from luminous flame to blue flame was observed together with a marked decrease of the flame length as the air flow rate Q_a was increased while keeping the fuel flow rate Q_f = 0.5L/min. We believe that as Q_a increases, the strength of the reverse flow and radial flow that are previously mentioned is increased. This enhances the fuel and air mixing in the area near the central jet that can be the reason why blue flame was observed for larger Q_a conditions.

In the case of (Q_f, Q_a) = (1.5L/min, 20L/min) shown in Fig. 4 (b), the reverse and radial flows same as those in Q_f = 0.5L/min case are observed. These reverse and radial flows are considered to enhance the fluid mixing near the central jet. Indeed, under this flow condition, a blue flame was observed in the combustor. However, compared to Fig.4 (a), the flow velocity downstream of the central nozzle is large. As Q_a increases, the velocity of the flow increases and the flame cannot be held close to the baffle-plate. This is considered to be the reason why the blow-off limit appears with relatively small Q_a condition.

In R75-s0 case shown in Fig. 5, the flow field largely differs with those observed in R60-s0 case. Reverse flow near the chamber sidewalls decreases, and a large reverse flow region is generated at the downstream of the central nozzle. The center-located reverse flow of the fluids supplied from the surrounding jet will impinge the central jet. An effective mixing of the fuel and air is expected in this area which will be discussed in the following paragraph. In addition to this mixing effect, the reverse flow helps the mixed fluid and flame to hold close to the baffle-plate. This can be the reason why a more stable flame was observed in R75-s0 case, compared with R60-s0 case.

In Fig. 6, the reaction rate, α, is plotted against the preferential generation rate of CO, γ, for the cases of R60-s0 and R75-s0. The flow rates are Q_f = 0.5L/min and Q_a = 30L/min. R60-s0 case shows relatively smaller α and larger γ that means an incomplete combustion is produced in the combustor. In the R75-s0 case, on the contrary, α increases and γ decreases, compared with the R60-s0 case. Thus, not only the reaction rate is increased, but also larger rate of complete combustion reaction is occurring in the combustor.

From these results, we can conclude that the generation of the reverse flow in the downstream of the central nozzle is more effective in enhancing the fuel and air mixing and producing a stable flame than the generation of the reverse flow near the sidewalls. Considering that these different flow structure can appear by slightly changing the value *R*, the distance between the central and surrounding nozzles, therefore, should be carefully decided so that a large reverse flow region in the center of the combustor be effectively formed in the parallel-type multijet case. The reverse flow may bring an additional effect of exhaust gas recirculation (EGR) to stabilize and enhance the combustion reactions.

3.2 Swirl-type multijet case

Figure 7 shows the blow-off conditions in the cases of R60-s20, R60-s40 and R75-s20. The results of R60-s0 and R75-s0 are additionally depicted in the figure for comparison. In R60-s20 case, the blow-off limit increases linearly as Q_f increases. In the R60-s40 and R75-s20 cases, the blow-off limit decrease slightly around Q_f = 0.75L/min, and shows a minimum value. It then increases with Q_f. The blow-off limit lines of all swirl-type cases cross the line of

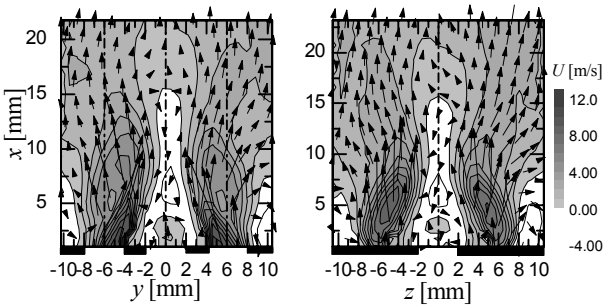

(a) *x*-*y* plane (b) *x*-*z* plane

Fig. 8 Streamwise velocity U contours and velocity vectors in R60-s20 case (Q_f = 1.5L/min and Q_a = 40L/min).

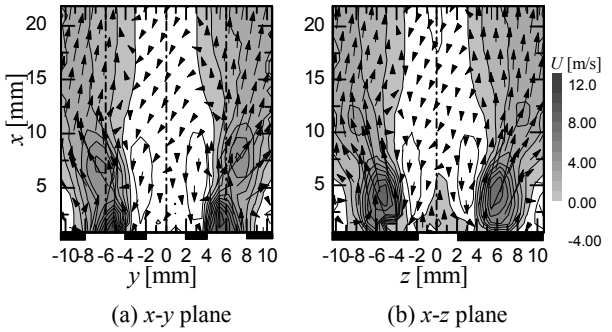

(a) *x*-*y* plane (b) *x*-*z* plane

Fig. 9 Streamwise velocity U contours and velocity vectors in R60-s40 case (Q_f = 1.5L/min and Q_a = 40L/min).

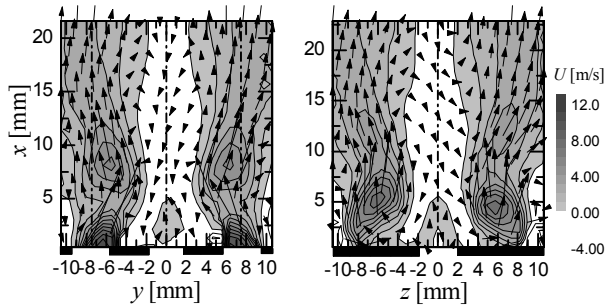

(a) *x*-*y* plane (b) *x*-*z* plane

Fig. 10 Streamwise velocity U contours and velocity vectors in R75-s20 case (Q_f = 1.5L/min and Q_a = 40L/min).

R75-s0 case at around $Q_f \cong$ 1.75L/min, and a larger blow-off limit is observed in these swirl cases for larger Q_f conditions.

Figures 8, 9, and 10 show the U contour maps and velocity vectors of each swirl case with the flow rate conditions of Q_f = 1.5L/min and Q_a = 40L/min. Focusing on the surrounding jet flows shown in Fig. 8 (a) presenting the *x*-*y* cross-sectional velocity distribution of R60-s20 case, one can see that the surrounding air jets first head toward the centerline in the area adjacent to the central nozzle outlet, and then flow outwards toward the chamber

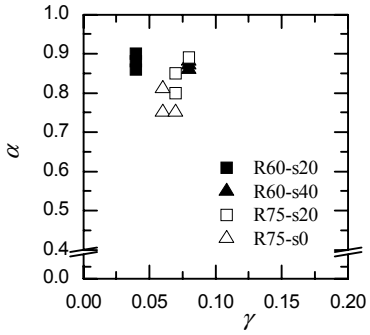

Fig. 11 Reaction rate, α, and preferential generation rate of CO, γ, in the cases of parallel-type multijet (Q_f = 1.5L/min and Q_a = 35L/min).

sidewalls in the downstream area. The latter flow is attributed to the centrifugal force caused by the swirl. Comparing Figs. 8 (a) and (b) with Figs. 4 (b-1) and (b-2), one can find that these flows decrease the strength of the reverse and radial flows that were observed near the sidewalls and baffle-plate, respectively. On the other hand, a reverse flow around the central region becomes dominant due to the swirl flow causing the decrease of the pressure in the area along the centerline.

In Figs. 9 and 10, velocity distributions similar to the R60-s20 case are observed in both figures. However, since *Sw* is larger in R60-s40 case than in R60-s20 case, greater centrifugal force works on the surrounding jets, and the jets flow toward the sidewalls in a shorter streamwise distance. A stronger reverse flow is, thus, observed at the centerline. In the case of R75-s20, the increase in R enhances the effects of the flow momentum difference obtained between the surrounding and central jets. This leads to the enhancement of the reverse flow generation in the area along the centerline. On the other hand, same as in R60-s40 case, the magnitude of the flow heading toward the centerline near the central nozzle exit is decreased compared with the R60-s20 case.

Figure 11 shows the plots of α versus γ in R60-s20, R60-s40 and R75-s20 cases. The results of R75-s0 with the flow rates of Q_f = 1.5L/min and Q_a = 40L/min are also plotted in the figure for comparison. The values of the R60-s20, R60-s40 and R75-s20 cases are located close with each other. Among them, the results of R60-s40 and R75-s20 cases are nearly identical, and the values of γ in R60-20 case are smaller than the other two cases. On the other hand, comparing these cases with the cases of R75-s0, α in the swirl-type cases shows a larger value. Furthermore, γ is nearly the same among the R60-s40, R75-s20 and R75-s0 cases.

Considering the velocity distributions previously discussed, we believe that the flow fields can be divided into two types in the swirl-type multijet case. The first type is the cases of R60-s40 and R75-s20 (cf. Figs. 9 and 10), where the swirl generates a relatively large reverse flow region at the chamber centerline that increases the fuel-air fluid mixing near the exit of the central nozzle. Such flow

structure seems similar with both two cases, except that the reverse flow at the centerline is weaker than in R75-s0 case.

The swirl, however, shows another significant influence on the flame characteristic, not shown in the PIV measurements. That is, the flame forms an axisymmetric shape and remains close to the chamber centerline, whereas the flame in the R75-s0 case happens to fluctuate in the spanwise direction in the chamber. This is considered to be attributed to the fact that the swirl reduces the radial flow flowing between the surrounding nozzles and helps the flame to move outwards toward the sidewalls. From these results, γ is larger in R60-s40 and R75-s20 cases than in R75-s0 case possibly attributed to the relatively poor fluid mixing at the exit of the central nozzle due to the weak reverse flow. However, since the flame remains stable near the centerline, a higher rate of complete combustion reaction is relatively easy to take place in the flame.

On the contrary, R60-s20 case shows a different flow structure and combustion performance (cf. Fig. 8). In this case, the flow of the surrounding jets heading toward the chamber centerline in the area adjacent to the central nozzle exit produces a strong interaction between the surround jets and the central jet. This largely increases the fuel-air fluid mixing in that area. The mixed gas will then spread widely in the chamber as it flows downstream owing to the swirl. These are considered to be the main reasons why larger α, smaller γ, and more stable combustion than the other swirl cases were observed in the R60-s20 case.

4. CONCLUSIONS

The combustion and flow characteristics of a baffle-plate-type millimeter-scale confined multijet were evaluated in this study. Blow-off condition, flow velocity, and gas components were measured for the parallel- and swirl-types of multijet. The influences of the distance between the central and surrounding nozzles, and the inclination angle of the surrounding nozzles were described. The main conclusions obtained are as follows:

(1) In the parallel-type multijet, a reverse flow was generated along the chamber centerline when the distance between the surrounding and central nozzles, R, was large. This led to the generation of a stable flame and a higher reaction rate with possible EGR effect. On the other hand, when R was small, no reverse flow was observed along the centerline, and the flame became unstable.

(2) In the swirl-type multijet, a reverse flow was observed at the chamber centerline. The area of the reverse flow was increased as the swirl number or R was increased. The swirl decreased the size of the reverse flow in some degree, compared with the parallel-type multijet. However, a stable flame with axisymmetric shape was obtained near the centerline. This led to a slight increase in the value of the preferential generation rate of CO and the reaction rate of the fuel.

MAIN SYMBOLS

d_i	Diameter of the central nozzle [mm]
d_o	Diameter of the surrounding nozzles [mm]
D	Diameter of the combustion chamber [mm]
G_a	Angular momentum [kg·m^2/s^2]
G_t	Translation momentum [kg·m/s^2]
L	Length of the combustion chamber [mm]
Q_a	Flow rate of the air jets [L/min]
Q_f	Flow rate of the fuel jet [L/min]
R	Distance between the surrounding and central nozzles [mm]
Re	Reynolds number
Sw	Swirl number
t_b	Thickness of the baffle plate [mm]
U	Streamwise velocity [m/s]
x	Coordinate in stream direction [mm]
y, z	Coordinates in radial direction [mm]

(Greeks)

α	fuel reaction ratio
γ	preferential generation rate of CO
θ	inclination angle of the surrounding nozzle
ϕ	Equivalent ratio

(Subscripts)

CH_4	value of the CH_4 component
CO	value of the CO component
CO_2	value of the CO_2 component

REFERENCES

[1] Choi, H. S., Katsumoto, Y., Nakabe, K. and Suzuki, K., An Experimental Investigation of Mixing and Combustion Characteristics on the Can-type Micro Combustor with a Multi-jet Baffle Plate, *Fluid Mechanics and its Applications Turbulent, Mixing and Combustion*, Vol. 70 (2002), pp. 367 – 375, Kluwer Academic Publisher.

[2] Woodfield, P. L., Nakabe, K. and Suzuki, K., Numerical Study for Enhancement of Laminar Flow Mixing using Multiple Confined Jets in a Micro-can Combustor, *Int. J. of Heat Mass Transfer*, Vol. 46 (2003), pp. 2655 – 2663.

[3] Yahagi, Y., Sekiguti, M. and Suzuki, K., Flow Structure and Flame Stability in a Micro Combustor with a Baffle Plate, *Applied Thermal Engineering*, Vol. 27 (2007), pp. 788 – 794.

[4] Tatsumi, K., Tanaka, M., Woodfield, P. L. and Nakabe, K., Swirl and Buoyancy Effects on Mixing Performance of a Baffle-Plate-Type Miniature Confined Multi-Jet, *Int. J. Heat and Fluid Flow*, Vol. 31 (2010), pp. 45 – 56.